Site-Selective Self-Assembly of Colloidal Photonic Crystals

By *Sanna Arpiainen,* Fredrik Jonsson, James R. Dekker, Gudrun Kocher, Worawut Khunsin, Clivia M. Sotomayor Torres,* and *Jouni Ahopelto*

A scalable method for site-selective, directed self-assembly of colloidal opals on topologically patterned substrates is presented. Here, such substrate contains optical waveguides which couple to the colloidal crystal. The site-selectivity is achieved by a capillary network, whereas the self-assembly process is based on controlled solvent evaporation. In the deposition process, a suspension of colloidal microspheres is dispensed on the substrate and driven into the desired crystallization sites by capillary flow. The method has been applied to realize colloidal crystals from monodisperse dielectric spheres with diameters ranging from 290 to 890 nm. The method can be implemented in an industrial wafer-scale process.

1. Introduction

Three-dimensional (3D) photonic crystals (PhCs) with optical cavities are promising components for signal processing and detector applications. New functionalities in various fields of applications are potentially viable by combining, for example, the increased light-matter interaction, cavity resonance modes, photonic band edge frequency, and large void space of the porous 3D network. To realize these functionalities on 3D PhCs, development of large scale processing methods to fabricate defect free crystals on pre-designed positions on a photonic chip and to control the frequency and mode structure of internal point defects and cavities, are needed. However, only few publications address the fabrication methods facilitating the integration of 3D PhCs with other photonic components.[1,2]

Two conceptually different approaches can be employed to generate the 3D PhC structures. One approach relies on controlled patterning and microfabrication methods such as focused ion beam milling,[3] direct laser writing by multiphoton polymerization,[4] robotic ink writing,[5] conventional[6] or holographic[7] lithography, or micromanipulation.[8] Most of these methods readily offer means for defect inscription inside the structure, but are limited either by the speed of processing or by the resolution, though in some cases these may improve in the future. The other approach is based on self-assembly of monodisperse colloidal spheres, featuring, e.g., gravitational sedimentation,[9] vertical deposition,[10] colloidal epitaxy,[11] electrophoresis,[12] molding into capillaries,[13] and the flow cell method.[14] These self-assembly techniques can be applied to form PhC structures with photonic band gaps ranging from deep UV to far IR frequencies, while being both fast and cost efficient. However, they cannot be directly employed to fabricate deterministic defects, for which they have to be complemented by lithographic means.[15,16]

In this paper, we present the capillary directed self-assembly (CDSA) method, which can be considered as a modification of the vertical deposition technique. In vertical deposition, a hydrophilic substrate is immersed into the colloidal suspension, and slowly withdrawn to form a thin meniscus at the liquid/vapor interface. The microspheres agglomerate on the meniscus with solvent evaporation and self-organize into a face centered cubic (fcc) lattice due to the strong attractive forces in the liquid necks between the drying spheres. In CDSA, instead of dipping the substrate into the suspension, a sub-microliter droplet of the suspension is dispensed into a reservoir well on the substrate as presented schematically in Figure 1. The colloidal microspheres are directed into the desired positions via capillary channels and self-assembled due to solvent evaporation and capillary force. The

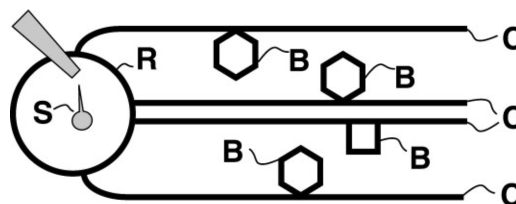

Figure 1. Schematic presentation (not in scale) of the CDSA substrate, also featuring the pipette head dispensing a droplet of suspension (S) into reservoir well (R). The suspension is directed via capillary channels (C) into adjacent opal basins (B).

[*] S. Arpiainen, Prof. J. Ahopelto
VTT Micro and Nanoelectronics
P.O. Box 1000, FIN-02044 VTT (Finland)
E-mail: sanna.arpiainen@vtt.fi

Dr. F. Jonsson, Dr. G. Kocher, Dr. W. Khunsin, Prof. C. M. Sotomayar Torres[+]
Tyndall National Institute, University College Cork
Lee Maltings, Cork (Ireland)

Dr. J. R. Dekker
VTT Center for MEMS and Heterogeneous integration
P.O. Box 1000, FIN-02044 VTT (Finland)

[+] Present addresses: Catalan Institute of Nanotechnology, Campus de Bellaterra, Edifici CM7, ES 08193 Bellaterra Barcelona (Spain) and Catalan Institute of Research and Advanced Studies (ICREA), 08010 Barcelona (Spain)

DOI: 10.1002/adfm.200801612

© 2009 WILEY-VCH Verlag GmbH & Co. KGaA, Weinheim
WILEY InterScience DISCOVER SOMETHING GREAT

ADVANCED FUNCTIONAL MATERIALS

major advantage introduced by CDSA over the former self-assembly methods is the full spatial selectivity of the opal growth, also resulting in negligible particle contamination of the substrate. The technological advantage of the method lies in the exploitation of the existing standard microelectronics or MEMS fabrication processes combined with directed self-assembly. Automated delivery of the suspension combined with fully controlled deposition environment could facilitate the up-scaling of CDSA to large scale production.

2. The CDSA Process

2.1. Substrates for CDSA

Two different substrate designs were used in the demonstration of the CDSA process. The simple (Type A) substrates consisted of reservoir wells (not shown) connected to capillary channels, further connected to rectangular opal basins as presented in Figure 2. The capillary channels were divided into sub-channels and the nominal sub-channel width was varied from 0.4 to 2 μm. Rectangular opal basins of 100 μm in length and 10 μm in width were located aside this channel. The distance from the reservoir well to the opal basin varied from 100 μm to 2 mm, and all the patterns were defined to a uniform depth of about 5 or 6 μm from the top surface.

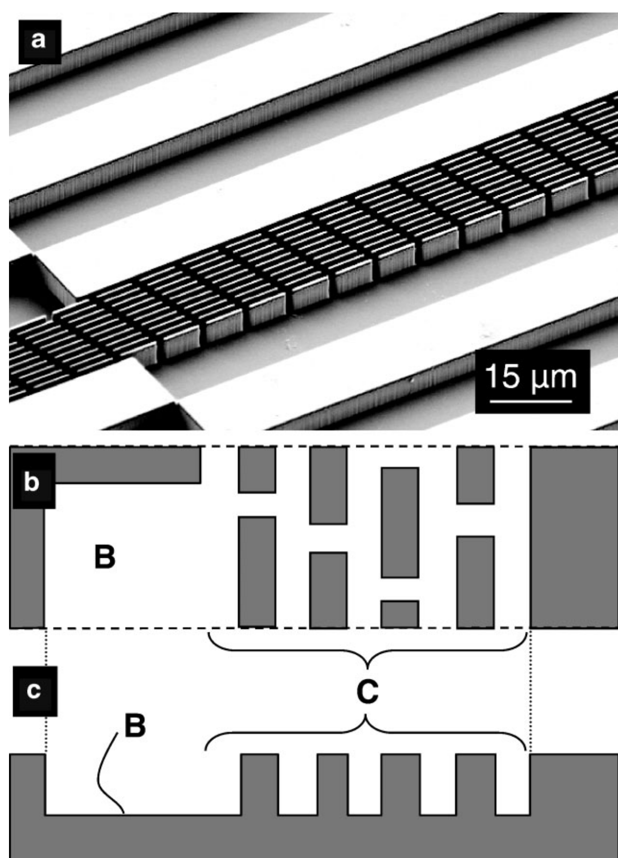

Figure 2. Type A substrate. a) SEM image, and b) top and c) cross-section schematics of the surface topology featuring the capillary channel (C) and the adjacent opal basin (B).

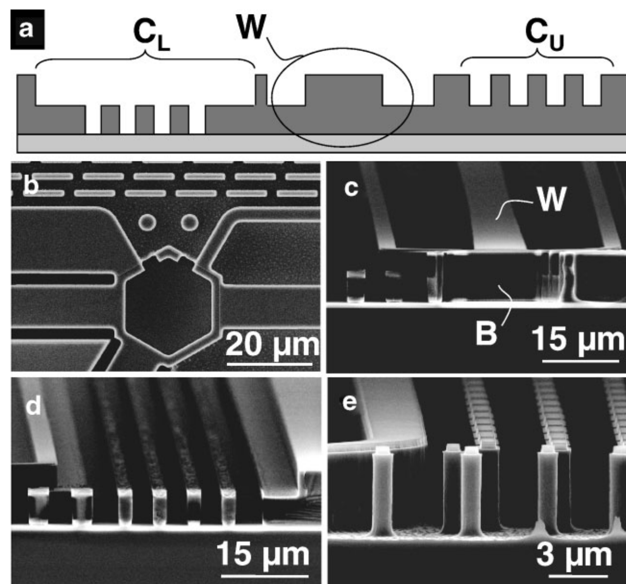

Figure 3. Type B SOI substrate. a) Schematics of the surface topology, featuring the lower (C_L) and upper (C_U) capillary channels and the ridge waveguide (W). b–d) SEM images of capillary channel(s) and adjacent opal basin after ICP etch. b) Top view of a 20 μm wide hexagonal opal basin, three connected waveguides and upper capillary channel. c) Cross-section view of another 20 μm wide hexagonal opal basin showing the connections from the capillary channels into the basin and the vertical interface between basin and waveguide. d) The lower and e) the upper capillary channel.

Substrates with opal basins integrated to optical waveguides (Type B) were defined on silicon-on-insulator (SOI) wafers and included capillary channels at two height levels for two step sedimentation. Opal basins defined through the 10 μm SOI film and the optical waveguides connected to these 20 μm wide hexagonal basins are shown in Figure 3. The upper capillary channels with nominal sub-channel width of 2 μm were etched to a depth of 4.5–5 μm on the upper part of the SOI film, together with the corresponding reservoir wells (not shown) for dispensing the suspension. The other, lower capillary channels, with a nominal sub-channel width of 3 μm reached from the midway of the SOI film down to the top of the buried oxide (BOX) film, giving the sub-channels a depth of typically 5 μm. These channels, as well as the corresponding reservoir areas, were designed to keep the dispersion in the lower half of the SOI film filling only the sub-channel volume between the 3 μm pillars from bottom to about half of the total height of the 10 μm SOI film. In both capillary channel systems, two distinct opal basins were connected to the capillaries, the first at 3 mm and the second at 9 mm distance from the reservoir well. Each opal basin was connected either to an upper channel only, or to both upper and lower channels.

2.1.1. Substrate Fabrication

Substrates were fabricated on *n*-type (100) bulk silicon wafers and on bonded SOI wafers with a 10 μm thick (100) SOI film on 1 μm thick BOX. The wafers were patterned using optical lithography

WILEY InterScience® DISCOVER SOMETHING GREAT

© 2009 WILEY-VCH Verlag GmbH & Co. KGaA, Weinheim

and the pattern was transferred into silicon in an inductively coupled plasma (ICP) etcher with fluorine chemistry. Instead of the standard pulsed Bosch ICP process, with sequential etch and passivation cycles, a continuous process with simultaneous etch and passivation was employed.[17] With a gradually decreasing platen bias power and ramping of the etch and passivation gas flow rates, trenches with optically smooth and vertical sidewalls were defined up to a depth of 5–6 μm in each run. Both single layer (Type A) and double layer (Type B) processes were employed. The double layer etch process was realized with two successive masks layers: a SiO_2 hard mask and a sacrificial resist mask. The first etch step was followed by an in situ oxygen plasma to remove the sacrificial mask and also the excess sidewall passivation polymers before initiating the second etch step. After etching, the fluorine polymer residues were removed by harsh plasma and wet chemical treatments. The Type B substrates were then thermally oxidized to reduce the surface roughness and provide optical cladding on the waveguides. The first 250 nm thick thermal oxide was grown at 1000°C (not oxidation) and subsequently removed in diluted HF to improve the edge profiles of the lower capillary channels. Another 250 nm thick SiO_2 film was then grown as the final substrate coating. Prior to the opal deposition, the substrates were hydrophilized in $NH_4OH/H_2O/H_2O_2$ 1:5:1 at 65 °C for 5–10 min.

2.2. Opal Deposition

Opal deposition is initiated by dispensing a small 0.2–0.8 μL droplet of suspension into the reservoir on the substrate, from where it is directed via unsealed capillaries into the opal basins. The process duration, from dispensing the droplet to the final drying of the dispersion, was usually about 10 min. The most crucial limiting parameter for the growth was found to be the evaporation rate of the suspension, determined by the process ambient relative humidity (RH) of the solvent in dispersion (water, ethanol, etc.) and by the temperature of the substrate and suspension. When the evaporation rate is too high, the deposition process is terminated by premature drying of the suspension in the capillary channels and the growth in the opal basins is ceased. The crucial level of the evaporation rate can also be tailored by the volume concentration of the spheres in the suspension, lower concentrations enabling higher evaporation rates. During the deposition, the process chamber RH at equilibrium was nominally 97%, but lower values, down to about 93%, could also be utilized while maintaining the atmosphere stability on the time scale of the deposition.[18] The best opal quality was usually obtained at the lowest applicable RH of 93%. However, deposition in another chamber with nominal RH of 75% resulted in severe drying of the suspension. The temperature of the chamber atmosphere, suspension, and substrate could be varied independently, but the best results were obtained in thermal equilibrium, i.e., when these coincided. Thus the process temperature, which determines the kinetic energy of the colloidal spheres, was limited by the process chamber temperature and could be varied in the range of 20–30 °C. The best crystals were obtained at highest temperatures.

3. Characterization of Opals

Scanning electron micrographs of silica opals crystallized by CDSA are presented in Figures 4 and 5. When comparing Figure 2a to Figures 4a and b representing the Type A substrate prior to and after the opal deposition, respectively, the high spatial selectivity of the method is evident. Opal deposition occurs only on structures physically connected to the capillary channel (Fig. 4a and b). Ideally, the opal thickness is determined by the substrate topology, as the trenches are filled up to the top due to the surface tension, and the lateral crystalline orientation is determined by the geometrical confinement of the opal basin. The capillary-force induced ordering, or minimization of the surface tension, also strongly favors the orientation of the dense hexagonal (111) surface at the drying interface.

The opals in Figure 4, originating from initial growth runs were deposited on Type A substrates under poorly controlled RH which often resulted in premature drying of the suspension. However, the crystalline order of the opals was usually good, which

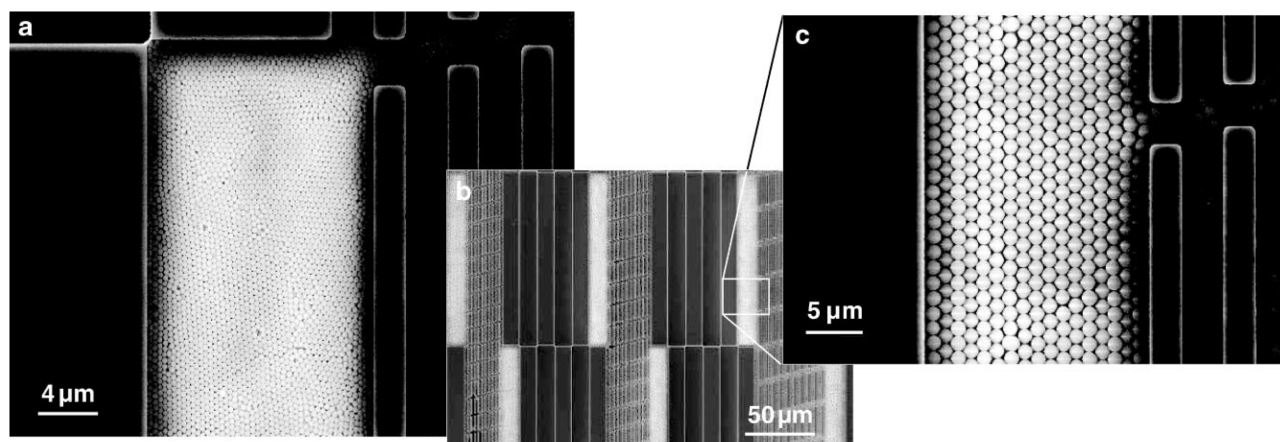

Figure 4. Scanning electron micrographs of opals deposited with CDSA on Type A substrates from a) small (∅ = 290 nm) and b–c) large (∅ = 890 nm) beads. The basins not connected to the capillary channels remain empty (compare to Fig. 1a).

© 2009 WILEY-VCH Verlag GmbH & Co. KGaA, Weinheim
WILEY InterScience DISCOVER SOMETHING GREAT

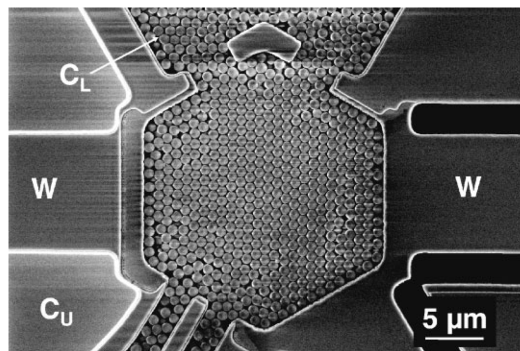

Figure 5. Scanning electron micrograph of an opal deposited from silica spheres ($\emptyset = 890$ nm) on a 20 µm wide and 10 µm deep hexagonal basin on a photonic chip (Type B). The capillary channel on the left (C_L) was used for bead delivery. Deposition was performed at 93% RH and at 30 °C. Waveguides (W) are optically connected to the opal, with end facets parallel to the edges of the basin. Due to the geometric mismatch between the 90° basin wall and the side of the fcc crystal with preferentially 45° edge or zigzag pattern, the first sphere layer is somewhat misplaced at the optical interface.

was verified by optical characterization. Domains of different lattice orientation with respect to the ΓK and ΓM directions were formed (Fig. 4a) in opals deposited from 10% w/w aqueous dispersion of small $\emptyset = 290$ nm silica spheres into a 10 µm wide basin. However, when the sphere size was larger (Figs. 4c and 5) the opals were usually well aligned with the basin geometry and instead of crystal domains, line and point defects were detected as crystal imperfections.

The opal deposition experiments on Type B substrates were performed at constant RH of 93–97%. These SOI substrates are passive photonic chips with single mode and multi mode ridge waveguides connected to the opal basins as shown in Figures 3b and 5. The space required by the waveguides, as well as the small dimensions of the opals in practical applications, set limitations to the geometry of the opening connecting the capillary channel to the opal basin, as the capillary channel cannot be placed close to the optical waveguides. However, as will be discussed in Section 4, the geometry of this connection is of great importance for the filling of the opal basins.

3.1. Optical Characterization

Optical reflectivity is an important measure of the crystalline quality of the opal. Instead of visualizing only the top surface, reflectance spectra provide information on the layer spacing and optical, or packing, density of the opal. Though it is not possible to distinguish between fcc (ABCABC stacking) and hexagonal close packed (hcp) (ABAB stacking) structures and their random combinations based on the reflectance spectra measured from the (111) surface, the formation of pure fcc lattice is energetically favored in evaporation-based ordering of colloidal spheres, when the growth direction is perpendicular to the surface, i.e., perpendicular to the (111) surface.[11] Reflectance spectra of opals with the first order Bragg reflection peak at the visible wavelength range were measured with a NanoSpec III spectrophotometer. A typical spectrum of an opal crystallite from a 15 µm area through a 10× magnifying lens (NA 0.33) is represented in Figure 6a. The opal was deposited on Type A substrate using silica beads with a diameter of 290 nm and refractive index n of 1.37. The first order Bragg reflection peak is located at 595 nm with a relative peak width $\Delta\lambda/\lambda$ below 6%, which is equivalent to the Γ-valley pseudogap with a theoretical width of 5.1%.[19] This, together with the 65% peak reflectivity, is interpreted to indicate to a good crystalline quality of the opal. The period of the Fabry–Perot fringes indicates an opal thickness of about 3.5 µm in the measured area. This is significantly less than the 5–6 µm depth of the structures on the substrate and indicates premature drying of the suspension.

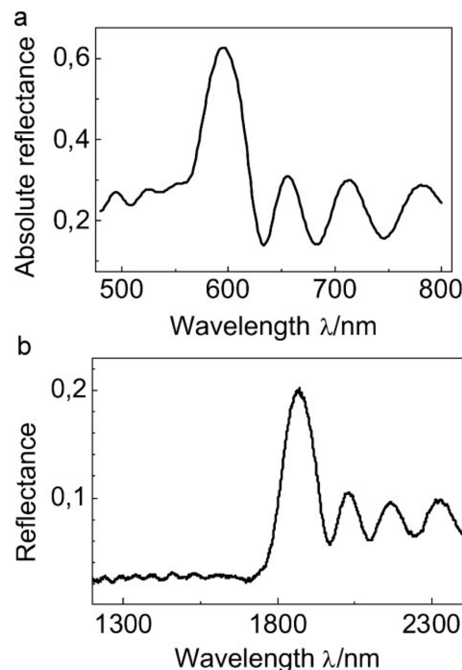

Figure 6. a) Measured reflectance from a 3.5 µm thick opal crystallite with the silica bead diameter $\emptyset = 290$ nm on Type A silicon substrate. Measurement area diameter was 15 µm. b) Measured IR reflectance from opal with silica bead diameter $\emptyset = 890$ nm. The opal was deposited on a 12 µm deep hexagonal opal basin of 20 µm in radius on Type B silicon substrate. The measurement area was 10 µm × 20 µm.

Figure 6b shows an infrared reflectance spectrum of an opal deposited from silica beads of 890 nm in diameter into Type B silicon substrates. The reflectance was measured in a Bruker FTIR Spectrophotometer, where the measurement area was reduced to a 10 µm × 20 µm spot to avoid spectral contribution from the surrounding silicon. The relative width $\Delta\lambda/\lambda$ of the first order Bragg reflection at 1.85 µm is less than 7%, again indicating rather good fcc order. The slight increase in $\Delta\lambda/\lambda$ may result from the contribution of the opal edges, where some disorder, also shown in Figure 5, is unavoidably introduced by a mismatch between the (111) packing and the vertical wall of the opal basin. The opal thickness of 12 µm determined from the Fabry–Perot fringes corresponds exactly to the depth of the basins on the silicon substrate confirmed by profilometry and is slightly larger than on the actual SOI substrates. Reflectance spectra of similar opals deposited on SOI substrates were strongly affected by the

© 2009 WILEY-VCH Verlag GmbH & Co. KGaA, Weinheim

1 μm BOX related reflectance maximum at around the same spectral position of the first order Bragg reflectance, which prevented reliable resolution. The opal transmission in ΓM direction was also measured through the waveguides coupled to the opals in Type B substrates. The optical loss when passing through the two waveguide/opal interfaces and a 15 μm long opal was measured to be around 8 dBm, which is roughly identical to the transmission of the structure in the case of an empty basin. This is in line with 3D numerical simulations, which indicate that there are no opal dispersion related spectral effects in the applicable measurement range (below 1.7 μm). Further details will be reported elsewhere.

4. Description of the CDSA Process

Based on the above results, the CDSA process can be divided into three strongly interacting processes; initial wetting of the capillaries by capillary flow, aggregation of the colloidal spheres by solvent evaporation, and simultaneous ordering of the spheres into a 3D crystal lattice in the basins.

Once the suspension is dispensed in the reservoir, it is driven into a capillary channel. The flow of the suspension is determined by the differential capillary pressure in the channel, which maintains the flow until complete wetting of the channel and the opal basins occurs. However, if the capillary pressure in the opal basin is much smaller than in the capillary channel and, furthermore, it is not compensated by the design of the connecting openings at their interface, the wetting of the opal basin will be hindered.[20] In Type A substrates, where the opal basin is essentially only a wider part of the channel, the capillary channels with the lowest capillary pressure gave the best results with respect to the wetting of the basins. In Type B substrates with identical 2 μm upper channels connected by 4 μm wide opening to the opal basin, there was essentially no wetting of the opal basins with any level of substrate hydrophilicity. Either the capillary flow was completely prohibited by weak hydrophilicity in the channels, or, at higher levels, the capillary pressure in the opal basins was too low compared to that in the channels. However, the nominally 3 μm wide lower channels in Type B substrates provided a wide operational range in surface hydrophilicity. The edge spiking illustrated in Figure 3d induced unintentional flow of the suspension from the 3 μm wide sub-channels at the bottom of the channel into the 50 μm wide and 5 μm thick open volume at the top of the channel. This introduced a channel with 3 μm sized bottom structure with high capillary pressure and strong capillary flow, perfect for the initial wetting of the channel, combined to upper part with rather low capillary pressure facilitating efficient flow of the suspension through the gate into the basins.

After the wetting phase, the transport of the suspension continues in order to replace the evaporated liquid. The evaporation rate is determined by the substrate geometry and by the RH of the solvent in the environment. Together with the volume fraction of the spheres in the suspension, the evaporation rate from the capillaries and from the opal basins determines the sphere aggregation rate into the opal basins. This rate has to be small enough to provide the spheres enough time to find the global energy minimum position in the opal lattice, and the optimum value thus also depends on the process temperature or the kinetic energy of the colloidal spheres.

As in vertical deposition, the ordering of colloidal spheres in CDSA is due to strong attractive interaction of the drying spheres, induced by the capillary force in the remaining liquid necks between the spheres.[21] In vertical deposition, the growth and ordering occur at the drying zone above the meniscus moving across the surface. In CDSA, there is no drying zone unambiguously connected to the aggregation and ordering of the spheres, as liquid transport may continue inside the aggregated spheres long after the sphere transport has ceased. However, the experimental data indicates that the requisite for the formation of highly ordered opal is the formation of such drying zone, due to high enough evaporation from the already ordered opals and possible capillary structures following the opal, obtained by a balance between sphere aggregation and drying. The best crystalline order in opals deposited on Type B substrates was indeed obtained when the chamber RH was reduced clearly below the equilibrium value of 97%, i.e., down to 93%. Another important factor affecting the quality of crystallization is the kinetic energy of the colloidal spheres. The kinetic energy has to be in balance with the deposition rate and the inter-sphere capillary force at the drying zone. Besides increasing the process temperature, additional kinetic energy can be provided to the spheres without affecting other components of the equilibrium by, e.g., introducing acoustic noise.[2]

5. Discussion

At the current state of the process development, the yield of the method is rather moderate. Typically most of the opals deposited by CDSA are crystalline, but the average crystallite size varies from deposition to deposition from a few to tens of micrometers. The yield of single crystalline opals perfectly aligned with ΓM direction parallel to the light propagation in the waveguides is related to the average crystallite size, typically only a few percent. We believe that the yield can be significantly improved by stabilizing and optimizing further the CDSA process. Possible improvements include vibration isolated environment, an enhanced process chamber with control over the process temperature and RH over a larger range and with better reproducibility, use of the above mentioned acoustic noise as a source of additional kinetic energy and, especially, microfluidics modeling to optimize the channel and connecting gate geometries.

After optimizing the process, wafer scale production can be easily implemented in a chamber with controlled temperature and RH, using an automated dispenser. With an aligned, small volume dispensing unit (matrix), the reservoirs and the capillary channel length and width can be optimized for each application to achieve minimal usage of space. In the production environment, the short process duration of about 10 min, and the small material consumption are also advantageous. The suggested route toward the large scale production of integrated 3D PhCs exploits the existing standard microelectronics or MEMS fabrication processes, also employed in the fabrication of the conventional photonic circuits, and combines them with the directed self-assembly on a controlled manner.

© 2009 WILEY-VCH Verlag GmbH & Co. KGaA, Weinheim
WILEY InterScience® DISCOVER SOMETHING GREAT

The combination of CDSA with graphoepitaxy to achieve full control over the ΓM–ΓK orientation and exact lattice positioning in (111) oriented opals is an attractive concept which could be easily realized also on a larger scale by patterning the template on the basin with standard UV lithography. For some applications of direct and inverted opals, like self-guiding[22] and superlensing,[23] where defect inscription is not relevant, the optimal direction of light propagation may not be parallel to the (111) surface. Though graphoepitaxial methods have proven extremely powerful in the generation of (100) oriented opals, e.g., in colloidal epitaxy[11] based on gravitational sedimentation and in electrophoretic deposition,[24] it cannot be taken as granted that a square pattern generated at the bottom of the well would actually generate a (100) oriented crystal in CDSA. Recent results with convective sedimentation, where self-assembly is also based on capillary necks instead of gravitational or electromagnetic field, have not been too promising due to the strong preference for the (111) surface at the air/liquid interface.[25] However, combining on-chip advances of CDSA with graphoepitaxial electrophoretic deposition by introducing a chip with integrated electrodes, capillaries, and opal templates might eventually provide an industrial scale self-aligned process with full control over the crystal orientation.

Though the current state of alignment precision of CDSA is sufficient for most sensor applications of opals, for mode structure tailoring required by photonic applications a complete control on the crystal orientation and lattice configuration is necessary, as well as the ability to generate controlled point or line defects inside the opal. The controlled defect inscription on self-assembled 3D opals has already been demonstrated using two different approaches that both could also be applied with CDSA. The use of direct-write techniques, or laser writing with two-photon polymerization, has been demonstrated to generate sub-micrometer line defects inside 3D opal with a full control over the defect position.[16] Another patterning approach is to deposit the opal in two steps, enabling patterning of the first opal before the deposition of the second opal film on top. However, from the multitude of methods developed for this patterning scheme, only electron-beam exposure of selected methyl 2-methylpropanoate (PMMA) beads[15] is suitable for point-defect or defect array inscription without disturbing the 3D symmetry and the order of the subsequently deposited second opal film. Alternatively, a thin 2D layer can be deposited at the interface,[26,27] and patterned by more scalable high resolution optical lithography if the exact position of spheres can be predetermined.

6. Conclusions

We demonstrated a scalable method, CDSA, for site-selective, directed self-assembly of colloidal opals on topologically patterned substrates. By employing the method, 3D opals were self-assembled into desired positions on a passive photonic chip, whereas other topological, strongly structured features on the substrate remained intact and clean from opals and residuals of the colloidal solution. We showed that it is possible to direct the suspension of large colloidal silica beads of ~1 μm in diameter to the crystallization sites confined by the walls of an optical cavity, and to self-assemble these large beads into an fcc opal with crystalline dimensions suitable for photonics integration. This is an important achievement, as the large sphere sizes are required to produce the full photonic band gap in silicon inverted crystals around the 1.55-μm wavelengths.

The crystal orientation of the opals deposited by CDSA was found to be fixed by the capillary force induced ordering to a (111) surface direction, and the orientation in ΓK–ΓM direction to be defined by the basin geometry. However, further process optimization is still required in order to increase the yield of defect-free, single-crystalline opals. The CDSA method can be improved by introducing additional energy to the colloidal spheres with, for example, acoustic vibrations or increased process temperature, and by optimizing the substrate geometry with respect to wetting and evaporation. Despite the work still to be done for optimizing the CDSA method, the demonstration of the 3D photonic crystal integration on passive photonic chip with potential for wafer scale processing is an important step towards the utilization of 3D photonic crystals in integrated optics.

Acknowledgements

This work was financed by EU-IST projects PHAT and PhOREMOST, by the Science Foundation Ireland grant no. 02/IN.1/172 and by Academy of Finland TULE Research Program. The SOI wafers were donated by Okmetic Ltd. The authors thank Prof. Rudolf Zentel's and Prof. Unger's groups (University of Mainz, Germany) from the synthesis and purification of the large silica spheres, and Ms. Merja Markkanen for substrate fabrication. Supporting Information is available online from Wiley InterScience or from the author.

Received: October 31, 2008
Revised: December 18, 2008
Published online:

[1] G. A. Ozin, S. M. Yang, H. Miguez, US Patent Application Publication **2004**, US2004/0053009 A1.
[2] G. Kocher, W. Khunsin, S. Arpiainen, J. Romero-Vivas, S. G. Romanov, J. Ye, B. Lange, F. Jonsson, R. Zentel, J. Ahopelto, C. M. Sotomayor Torres, *Solid State Electr.* **2007**, *51*, 333.
[3] C. C. Cheng, A. Scherer, R.-C. Tyan, Y. Fainman, G. Witzgall, E. Yablanovitch, *J. Vac. Sci. Technol. B Microelectron. Nanometer Struct. (USA)* **1997**, *15*, 2764.
[4] H. B. Sun, S. Matsuo, H. Misawa, *Appl. Phys. Lett.* **1999**, *74*, 786.
[5] G. M. Gratson, M. J. Xu, J. A. Lewis, *Nature* **2004**, *428*, 386.
[6] S.-Y. Lin, J. G. Fleming, D. L. Hetherington, B. K. Smith, R. Biswas, K. M. Ho, M. M. Sigalas, W. Zubrzycki, S. R. Kurth, J. Bur, *Nature* **1998**, *394*, 251.
[7] V. Berger, O. GauthierLafaye, E. Costard, *J. Appl. Phys.* **1997**, *82*, 60.
[8] F. Garcia-Santamaria, H. T. Miyazaki, A. Urquia, M. Ibisate, M. Belmonte, N. Shinya, F. Meseguer, C. Lopez, *Adv. Mater.* **2002**, *14*, 1144.
[9] K. E. Davis, W. B. Russel, W. J. Glantschnig, *Science* **1989**, *245*, 507.
[10] a) P. Jiang, J. F. Bertone, K. S. Hwang, V. L. Colvin, *Chem. Mater.* **1999**, *11*, 2132. b) Z. Z. Gu, A. Fujishima, O. Sato, *Chem. Mater.* **2002**, *14*, 760.
[11] A. van Blaaderen, R. Ruel, P. Wiltzius, *Nature (London)* **1997**, *385*, 321.
[12] a) M. Trau, D. A. Saville, I. A. Aksay, *Science* **1996**, *272*, 706. b) M. Holgado, F. García-Santamaría, A. Blanco, M. Ibisate, A. Cintas, H. Míguez, C. J. Serna, C. Molpeceres, J. Requena, A. Mifsud, F. Meseguer, C. López, *Langmuir* **1999**, *15*, 4701.
[13] H. Míguez, S. M. Yang, N. Tétreault, G. A. Ozin, *Adv. Mater.* **2002**, *14*, 1805.
[14] E. Kim, Y. Xia, G. M. Whitesides, *Adv. Mater.* **1996**, *8*, 245.

© 2009 WILEY-VCH Verlag GmbH & Co. KGaA, Weinheim

[15] F. Jonsson, C. M. Sotomayor Torres, J. Seekamp, M. Schniedergers, A. Tiedemann, J. Ye, R. Zentel, *Microelectr. Eng.* **2005**, *78–79*, 429.
[16] a) W. M. Lee, S. A. Pruzinsky, P. V. Braun, *Adv. Mater.* **2002**, *14*, 271. b) Y. H. Jun, C. A. Leatherdale, D. J. Norris, *Adv. Mater.* **2005**, *17*, 1908.
[17] K. Solehmainen, T. Aalto, J. Dekker, M. Kapulainen, M. Harjanne, P. Heimala, *J. Opt. A: Pure Appl. Opt.* **2006**, *8*, S455–S460.
[18] See supplementary information.
[19] Calculations by M. I. T. Photonic Bands software: S. G. Johnson, J. D. Joannopoulos, *Opt. Exp.* **2001**, *8*, 173.
[20] a) E. Delamarche, A. Bernard, H. Schmid, A. Bietsch, B. Michel, H. Biebuyck, *J. Am. Chem. Soc.* **1998**, *120*, 500. b) D. Juncker, H. Schmid, U. Drechsler, H. Wolf, M. Wolf, B. Michel, N. de Rooij, E. Delamarche, *Anal. Chem.* **2002**, *74*, 6139.
[21] C. Fustin, G. Glasser, H. W. Spiess, U. Jonas, *Langmuir* **2004**, *20*, 9114.
[22] R. Iliew, C. Etrich, F. Lederer, *Opt. Exp.* **2005**, *13*, 7076.
[23] a) K. Ren, Z.-Y. Li, X. B. Ren, S. Feng, B. Cheng, D. Zhang, *Phys. Rev. B* **2007**, *75*, 115108. b) T. Ochiai, J. Sánchez-Dehesa, *Phys. Rev. B* **2001**, *64*, 245113.
[24] N. V. Dziomkina, M. A. Hempenius, G. J. Vancso, *Adv. Mater.* **2005**, *17*, 237.
[25] J. P. Hoogenboom, C. Rétif, E. de Bres, M. van de Boer, A. K. van Langen-Suurling, J. Romijn, A. van Blaaderen, *Nano Lett.* **2004**, *4*, 205.
[26] a) E. Palacios-Lidón, J. F. Galisteo-López, B. H. Juárez, C. López, *Adv. Mater.* **2004**, *16*, 341. b) N. Tetreault, A. Mihi, H. Miguez, I. Rodriguez, G. A. Ozin, F. Meseguer, V. Kitaev, *Adv. Mater.* **2004**, *16*, 346.
[27] a) N. Tetreault, A. C. Arsenault, A. Mihi, S. Wong, V. Kitaev, I. Manners, H. Miguez, G. A. Ozin, *Adv. Mater.* **2005**, *17*, 1912. b) E. Vekris, V. Kitaev, G. von Freymann, D. D. Perovic, J. S. Aitchison, G. A. Ozin, *Adv. Mater.* **2005**, *17*, 1269. c) Q. F. Yan, Z. C. Zhou, X. S. Zhao, S. J. Chua, *Adv. Mater.* **2005**, *17*, 1917.

© 2009 WILEY-VCH Verlag GmbH & Co. KGaA, Weinheim
WILEY InterScience® DISCOVER SOMETHING GREAT